Towards stellar effective temperatures and diameters at 1 per cent accuracy for future surveys

L. Casagrande,[1]⋆† L. Portinari,[2] I. S. Glass,[3] D. Laney,[4] V. Silva Aguirre,[5] J. Datson,[2] J. Andersen,[6] B. Nordström,[6] J. Holmberg,[6] C. Flynn[7] and M. Asplund[1]

[1]*Research School of Astronomy and Astrophysics, Mount Stromlo Observatory, The Australian National University, ACT 2611, Australia*
[2]*Department of Physics and Astronomy, Tuorla Observatory, University of Turku, FI-20014 Turku, Finland*
[3]*South African Astronomical Observatory, PO Box 9, Observatory 7935, South Africa*
[4]*Bell Observatory, Western Kentucky University, Warren County KY 42274, USA*
[5]*Stellar Astrophysics Centre, Department of Physics and Astronomy, Aarhus University, Ny Munkegade 120, DK-8000 Aarhus C, Denmark*
[6]*Niels Bohr Institute, Copenhagen University, Juliane Maries Vej 30, DK-2100 Copenhagen, Denmark*
[7]*Centre for Astrophysics and Supercomputing, Swinburne University of Technology, VIC 3122, Australia*

ABSTRACT

The apparent size of stars is a crucial benchmark for fundamental stellar properties such as effective temperatures, radii and surface gravities. While interferometric measurements of stellar angular diameters are the most direct method to gauge these, they are still limited to relatively nearby and bright stars, which are saturated in most of the modern photometric surveys. This dichotomy prevents us from safely extending well-calibrated relations to the faint stars targeted in large spectroscopic and photometric surveys. Here, we alleviate this obstacle by presenting South African Astronomical Observatory near-infrared *JHK* observations of 55 stars: 16 of them have interferometric angular diameters and the rest are in common with the 2 Micron All Sky Survey (2MASS, unsaturated) data set, allowing us to tie the effective temperatures and angular diameters derived via the infrared flux method to the interferometric scale. We extend the test to recent interferometric measurements of unsaturated 2MASS stars, including giants, and the metal-poor benchmark target HD122563. With a critical evaluation of the systematics involved, we conclude that a 1 per cent accuracy in fundamental stellar parameters is usually within reach. Caution, however, must be used when indirectly testing a $T_{\rm eff}$ scale via colour relations as well as when assessing the reliability of interferometric measurements, especially at submilliarcsec level. As a result, rather different effective temperature scales can be compatible with a given subset of interferometric data. We highlight some caveats to be aware of in such a quest and suggest a simple method to check against systematics in fundamental measurements. A new diagnostic combination seismic radii with astrometric distances is also presented.

Key words: techniques: interferometric – techniques: photometric – stars: fundamental parameters – infrared: stars.

1 INTRODUCTION

Stellar angular diameters are crucial to correctly characterizing the basic properties of stars. First, the effective temperature $T_{\rm eff}$ is defined as the temperature of a blackbody with the same luminosity per unit surface as the star. Thus, if the angular diameter is measured, the determination of $T_{\rm eff}$ only requires the additional knowledge of the bolometric flux. Secondly, if the parallax is sufficiently well known, then it is possible to derive the star's intrinsic radius, competing with the radii obtained from eclipsing binaries to constrain stellar models (e.g. Andersen 1991; Torres, Andersen & Giménez 2010, and references therein).

Interferometric measurements of stellar angular diameters have a long history (Michelson & Pease 1921; Pease 1931; Brown & Twiss 1958), although it was only with Hanbury Brown, Davis & Allen (1974) that an extensive survey was carried out and used to calibrate empirically the effective temperature scale for early-type stars (Code et al. 1976). This campaign has continued throughout

⋆ E-mail: luca.casagrande@anu.edu.au
† Stromlo Fellow.

the years with increasingly sophisticated instrumentations both in the optical and infrared (e.g. SUSI: Davis & Tango 1986; Davis et al. 2011; Mark III: Mozurkewich et al. 1991; NPOI: Nordgren et al. 1999; IOTA: Dyck et al. 1996; PTI: Colavita et al. 1999). Recently, baselines exceeding 200 and 300 m have been achieved on VLTI and CHARA, respectively, yielding measurements of angular diameters for dwarfs and subgiants to a precision of ∼1 per cent or better (e.g. Kervella et al. 2003a; Huber et al. 2012; White et al. 2013). Although the accuracy might be lower, the aforementioned uncertainty translates to about 30 K at solar T_{eff}.

Arguably, the second most direct method to determine effective temperatures after interferometry is the infrared flux method (IRFM), a photometric technique originally devised to indirectly obtain angular diameters to a precision of a few per cent, and to compete with intensity interferometry should a good flux calibration be achieved (Blackwell & Shallis 1977; Blackwell, Shallis & Selby 1979; Blackwell, Petford & Shallis 1980). Casagrande, Portinari & Flynn (2006) and Casagrande et al. (2010) have updated the IRFM temperature scale, taking full advantage of the homogeneous near-infrared photometry of the 2 Micron All Sky Survey (2MASS), and of the extant accuracy in the photometric zero-points and absolute flux calibration (Cohen, Wheaton & Megeath 2003; Bohlin 2007). The new IRFM scale is in agreement with various spectroscopic ones (especially for solar-type stars; e.g. Valenti & Fischer 2005; Feltzing & Bensby 2008; Sousa et al. 2011) but about 100 K hotter than a number of older photometric scales (e.g. Alonso, Arribas & Martinez-Roger 1996b; Ramírez & Meléndez 2005b) including the one adopted in the Geneva–Copenhagen Survey, currently the largest and most complete census of long-lived stars in the solar neighbourhood (Nordström et al. 2004; Holmberg, Nordström & Andersen 2007, 2009).

Far from being a technicality, a systematic shift of +100 K in effective temperature implies a shift of about +0.1 dex on spectroscopically derived metallicities (e.g. Meléndez et al. 2010b). This shifts the peak of the metallicity distribution function in the solar neighbourhood from the historically accepted value of about −0.1 dex to roughly solar metallicity (Casagrande et al. 2011), with a number of consequences for Galactic chemical evolution models as well as for interpreting the Sun in a Galactic context (e.g. Wielen, Fuchs & Dettbarn 1996; Pagel 1997; Matteucci 2003; Asplund et al. 2009). A sound setting of the T_{eff} scale is crucial also for other reasons, e.g. in comparison with theoretical stellar models or to derive absolute abundances.

The zero-point of the Casagrande et al. (2010) IRFM scale was secured using solar twins, i.e. stars spectroscopically selected to be virtually identical to the Sun (Meléndez & Ramírez 2007; Meléndez et al. 2009; Ramírez, Meléndez & Asplund 2009); other, independent spectroscopic analyses of candidate solar twins also favour the hotter T_{eff} scale (Datson, Flynn & Portinari 2012, 2014; King, Boesgaard & Schuler 2005). The new scale has been tested in a number of studies, and with different approaches: with the colours of the Sun as derived from solar-like stars with the model independent line-depth-ratio technique (Casagrande et al. 2012; Ramírez et al. 2012), matching the theoretical solar isochrone to the open cluster M67 (VandenBerg, Casagrande & Stetson 2010; Pinsonneault et al. 2012) and with *Hubble Space Telescope* (*HST*) absolute spectrophotometry in the metal-poor regime (Casagrande et al. 2010).

However, the key test remains the comparison to angular diameters from direct interferometric measurements. So far, this was impeded by virtually zero overlap between stars with high-precision interferometric data and (unsaturated) 2MASS photometry, which is at the base of any modern implementation of the IRFM. In

Casagrande et al. (2010), an indirect comparison was performed by deriving angular diameters via optical colour–metallicity–T_{eff} and colour–magnitude–metallicity–bolometric flux relations, and the comparison to interferometry proved excellent. Although the optical relations were calibrated on the sample stars defining the IRFM scale, the comparison did not rely *directly* on the IRFM (see also discussion in Casagrande 2008).

Here, we overcome this major limitation and perform a direct, potentially conclusive test running the IRFM on 16 bright stars having angular diameter measurements. The trivial option of transforming existing near-infrared photometry of nearby stars into the 2MASS system is suboptimal (see Section 3), and thus we resort to new dedicated *JHK* photometry of nearby stars measured at the South African Astronomical Observatory (SAAO). The two IRFM scales (SAAO and 2MASS based) are tied together via 38 stars in common between the two systems.

While in this work we concentrate on stars with interferometric diameters above and around 1 mas, the increasing capabilities of CHARA (especially with the PAVO beam combiner; Ireland et al. 2008) and repeated, careful observations are now pushing the limit for reliable angular diameters down to ∼0.5 mas (White et al. 2013). This finally allows us to target stars having good 2MASS photometry and directly test a number of effective temperature scales as well as other interferometric measurements (Huber et al. 2012). Thus, this is the first time the 2MASS effective temperature and absolute flux scale is tested with high-precision interferometric angular diameters.

The plan of this paper is as follows. In Section 2, we present the near-infrared photometry measured from SAAO. In Section 3, we briefly recall the basic principles of the IRFM and derive the fundamental parameters of the sample stars, which we test against interferometric measurements in Section 4. In Section 5, we discuss the zero-point of the Geneva–Copenhagen Survey scale and of interferometric data. A simple exercise to highlight systematics and test the internal consistency of fundamental measurements is laid out. As it is now possible to estimate stellar radii from asteroseismic scaling relations, in Section 6 we present a new approach to gauge the angular diameter and effective temperature scale by coupling parallaxes with asteroseismology. In Section 7, we draw our conclusions.

2 NEAR-INFRARED SAAO OBSERVATIONS

The SAAO *JHK* photometric system was established by Glass (1974) and its accuracy and zero-points refined and improved over the years by Carter (1990) and Carter & Meadows (1995). Photometric observations were carried using the MkII IRP on the SAAO 0.75 m telescope, typically with a diaphragm size of 36 arcsec and with a fixed chopping amplitude of about 180 arcsec on a north–south line. Standard stars from the Carter list were observed roughly every hour.

SAAO photometry for the full sample is reported in Table 1. Around two thirds of the stars have double or multiple observations, and for them, we list average magnitudes and corresponding 1σ scatter. Based on the latter, we estimate typical photometric errors to be within 0.01−0.02 mag in all three bands (consistent with Carter 1990) and assume this value for stars having only one measurement.

For our sample stars having also accurate 2MASS photometry, the average difference between the two systems (2MASS−SAAO) is −0.047 ± 0.023 mag in *J*, −0.011 ± 0.024 mag in *H* and −0.032 ± 0.016 mag in *K*. These are, within the small colour range covered by our sample, in very good agreement with the

Table 1. Photometry and adopted parameters of sample stars.

HD	HIP	J	H	K	V	$B-V$	$V-R_C$	$V-I_C$	Ref.	$\log g$	[Fe/H]
30652	22449	2.380	2.130	2.104	3.190	0.460	0.270	0.525	B90	4.29[a]	−0.02[b]
38973	27244	5.615	5.304	5.259	–	–	–	–	–	4.39[b]	0.00[b]
39587	27913	3.387	3.035	2.988	–	–	–	–	–	4.47[b]	−0.12[b]
48737	32362	2.574 ± 0.003	2.323 ± 0.002	2.291 ± 0.002	–	–	–	–	–	3.83[b]	0.19[b]
52298	33495	6.003	5.748	5.695	–	–	–	–	–	4.37[b]	−0.30[b]
56537	35350	3.390 ± 0.011	3.309 ± 0.021	3.262 ± 0.071	–	–	–	–	–	3.90[c]	−0.10[c]
58192	35884	5.991	5.712	5.674	–	–	–	–	–	4.38[b]	−0.22[b]
69655	40438	5.575	5.265	5.219	–	–	–	–	–	4.40[b]	−0.20[b]
71334	41317	6.670 ± 0.007	6.301 ± 0.018	6.251 ± 0.003	7.809	0.664	0.367	0.714	R12	4.45[b]	−0.05[b]
75289	43177	5.375	5.108	5.054	–	–	–	–	–	4.32[b]	0.21[b]
75732	43587	4.576 ± 0.015	4.132 ± 0.003	4.069 ± 0.006	–	–	–	–	–	4.45[a]	0.31[a]
76151	43726	4.894 ± 0.022	4.553 ± 0.011	4.499 ± 0.005	6.000	0.670	0.360	0.695	B90	4.43[b]	0.03[b]
78534	44935	7.591 ± 0.013	7.236 ± 0.011	7.188 ± 0.015	8.688	0.654	0.345	0.684	R12	4.41[d]	0.07[d]
78660	44997	7.196	6.843	6.787	8.325	0.666	0.344	0.685	R12	4.39[b]	−0.03[b]
82943	47007	5.517	5.204	5.156	–	–	–	–	–	4.38[b]	0.30[b]
83683	47468	6.056	5.777	5.755	–	–	–	–	–	4.29[b]	−0.18[b]
86226	48739	6.860 ± 0.013	6.548 ± 0.011	6.489 ± 0.001	–	–	–	–	–	4.45[b]	0.00[b]
87359	49350	6.293 ± 0.014	5.927 ± 0.012	5.859 ± 0.011	–	–	–	–	–	4.42[b]	0.05[b]
88072	49756	6.432 ± 0.002	6.110 ± 0.010	6.049 ± 0.001	7.525	0.644	0.349	0.672	R12	4.45[b]	0.01[b]
91638	51784	5.725	5.439	5.397	–	–	–	–	–	4.30[b]	−0.20[b]
92719	52369	5.674	5.362	5.286	–	–	–	–	–	4.48[b]	−0.15[b]
93372	52535	5.397	5.148	5.112	–	–	–	–	–	4.31[b]	0.05[b]
94690	53424	7.056 ± 0.012	6.697 ± 0.011	6.622 ± 0.012	–	–	–	–	–	4.35[b]	0.25[b]
96700	54400	5.451 ± 0.026	5.101 ± 0.023	5.057 ± 0.021	6.530	0.600	0.340	0.670	C80	4.32[b]	−0.29[b]
97603	54872	2.277	2.229	2.201	–	–	–	–	–	3.90[c]	0.06[c]
101805	57092	5.560 ± 0.002	5.297 ± 0.002	5.245 ± 0.006	6.471	0.524	0.295	0.573	M89	4.29[b]	0.11[b]
102870	57757	2.641 ± 0.010	2.356 ± 0.007	2.308 ± 0.004	3.600	0.550	0.320	0.610	B90	4.22[a]	0.21[b]
103975	58380	5.814 ± 0.006	5.524 ± 0.007	5.483 ± 0.002	6.766	0.522	0.298	0.592	M89	4.30[b]	−0.03[b]
107692	60370	5.631 ± 0.028	5.302 ± 0.001	5.245 ± 0.010	6.703	0.651	0.349	0.674	R12	4.44[b]	0.20[b]
114174	64150	5.670 ± 0.018	5.299 ± 0.004	5.249 ± 0.005	6.761	0.688	0.349	0.694	R12	4.38[b]	0.05[b]
114853	64550	5.774 ± 0.001	5.411 ± 0.002	5.361 ± 0.010	–	–	–	–	–	4.46[b]	−0.16[b]
115169	64713	8.111 ± 0.005	7.769 ± 0.005	7.720 ± 0.017	9.250	0.648	0.355	0.690	R12	4.52[d]	−0.01[d]
118098	66249	3.161 ± 0.026	3.096 ± 0.021	3.077 ± 0.021	3.380	0.110	0.062	0.122	C80	4.02[c]	0.16[c]
121560	68030	5.196 ± 0.003	4.894 ± 0.003	4.858 ± 0.016	–	–	–	–	–	4.34[b]	−0.30[b]
131977	73184	3.841 ± 0.003	3.240 ± 0.007	3.146 ± 0.003	5.760	1.060	0.650	1.180	C86	4.76[a]	0.31[b]
132301	73383	5.718 ± 0.003	5.483 ± 0.002	5.453 ± 0.003	6.582	0.471	0.276	0.540	M89	4.34[b]	−0.03[b]
138573	76114	6.102 ± 0.009	5.742 ± 0.010	5.683 ± 0.006	–	–	–	–	–	4.41[b]	−0.04[b]
141795	77622	3.489 ± 0.015	3.437 ± 0.001	3.420 ± 0.003	3.710	0.150	0.065	0.129	C80	4.24[c]	0.23[c]
142331	77883	7.556 ± 0.010	7.194 ± 0.010	7.149 ± 0.012	8.727	0.681	0.368	0.719	R12	4.39[d]	0.04[d]
142860	78072	2.961 ± 0.023	2.685 ± 0.024	2.647 ± 0.013	–	–	–	–	–	4.18[a]	−0.14[b]
143436	78399	6.943 ± 0.004	6.609 ± 0.027	6.564 ± 0.018	–	–	–	–	–	4.28[e]	0.00[e]
145825	79578	5.436	5.095	5.058	6.533	0.678	0.352	0.699	R12	4.47[b]	0.12[b]
146233	79672	4.391 ± 0.016	4.057 ± 0.016	4.006 ± 0.015	5.510	0.650	0.357	0.691	R12	4.45[d]	0.05[d]
153458	83181	6.880 ± 0.005	6.538 ± 0.012	6.483 ± 0.009	–	–	–	–	–	4.42[b]	0.07[b]
157338	85158	5.878 ± 0.032	5.565 ± 0.005	5.508 ± 0.005	–	–	–	–	–	4.36[b]	−0.17[b]
157347	85042	5.118 ± 0.005	4.760 ± 0.012	4.708 ± 0.005	6.287	0.669	0.364	0.707	R12	4.42[b]	0.03[b]
159063	85799	6.095	5.834	5.800	–	–	–	–	–	4.26[b]	0.22[b]
164259	88175	3.921 ± 0.010	3.718 ± 0.015	3.691 ± 0.013	4.620	0.390	0.227	0.452	B90	4.08[b]	−0.08[b]
167060	89650	7.842 ± 0.004	7.504 ± 0.003	7.458 ± 0.008	8.943	0.644	0.354	0.679	R12	4.48[d]	0.02[d]
173667	92043	3.352	3.108	3.062	–	–	–	–	–	3.98[a]	−0.01[b]
177724	93747	2.938 ± 0.012	2.917 ± 0.004	2.880 ± 0.014	–	–	–	–	–	3.74[f]	−0.10[f]
182572	95447	3.958 ± 0.023	3.595 ± 0.028	3.504 ± 0.002	5.143	0.769	0.381	0.740	R12	4.32[a]	0.40[a]
184509	96370	5.760 ± 0.014	5.446 ± 0.024	5.400 ± 0.014	–	–	–	–	–	4.32[b]	−0.19[b]
189931	98813	5.839 ± 0.006	5.511 ± 0.015	5.458 ± 0.013	–	–	–	–	–	4.45[b]	0.01[b]
194640	100925	5.390 ± 0.010	5.009 ± 0.012	4.945 ± 0.012	6.615	0.730	0.392	0.762	C80	4.48[b]	−0.01[b]

Notes. Source of Johnson–Cousins photometry: Cousins (1980), Celis (1986), Menzies et al. (1989), Bessell (1990), Ramírez et al. (2012). Adopted stellar parameters: [a]Valenti & Fischer (2005); [b]Casagrande et al. (2011); [c]Takeda et al. (2009); [d]Ramírez et al. (2012); [e]King et al. (2005); [f]Gray et al. (2003).

updated transformations of Carpenter (2001).[1] Note though that no transformation between any of the photometric systems is done in this work: for the sake of the IRFM is in fact more robust to work directly with physical quantities (i.e. to implement the proper filter transmission curves, zero-points and absolute fluxes to translate magnitudes into fluxes) rather than converting magnitudes between different photometric systems, as explained later in more detail.

[1] http://www.astro.caltech.edu/~jmc/2mass/v3/transformations

3 FUNDAMENTAL PARAMETERS FROM THE INFRARED FLUX METHOD

The IRFM, an elegant and almost model-independent photometric technique for determining angular diameters and effective temperatures, has been implemented by various authors over the years (e.g. Blackwell & Shallis 1977; Blackwell, Shallis & Selby 1979; Blackwell et al. 1980; Bell & Gustafsson 1989; Blackwell & Lynas-Gray 1994; Alonso, Arribas & Martinez-Roger 1996a; Ramírez & Meléndez 2005a; Casagrande et al. 2006, 2010; González Hernández & Bonifacio 2009). While we refer to the aforementioned papers for a detailed description of the method, we briefly recall the key points relevant for this work.

The IRFM relies on the ratio between the bolometric flux ($\mathcal{F}_{bol}$) and the infrared monochromatic flux ($\mathcal{F}_{IR}$) of a star measured on the Earth. This ratio is compared to the one defined on a stellar surface element as follows:

$$\frac{\mathcal{F}_{bol}(\text{Earth})}{\mathcal{F}_{IR}(\text{Earth})} = \frac{\sigma T_{eff}^4}{\mathcal{F}_{IR}(\text{model})}. \tag{1}$$

Since T_{eff} is the only unknown quantity, it can be readily obtained. The crucial advantage of this procedure over other photometric techniques is that, at least for spectral types earlier than $\sim$M0, near-infrared photometry of stars samples the Rayleigh–Jeans tail of their spectrum, a region largely dominated by the continuum (but see Blackwell, Lynas-Gray & Petford 1991 for a discussion of the importance of H$^-$ opacity), with a roughly linear dependence on T_{eff} and very little affected by other stellar parameters, such as metallicity and surface gravity (as extensively tested in literature; e.g. Alonso et al. 1996a; Casagrande et al. 2006, 2010), and nearly free from non-local thermodynamic equilibrium (NLTE) and granulation effects (Asplund & García Pérez 2001; Casagrande 2009). The method (equation 1) yields *self-consistently* the effective temperature and bolometric flux of a star, from which its angular diameter (θ) can be trivially derived $\mathcal{F}_{bol}(\text{Earth}) = (\theta/2)^2 \sigma T_{eff}^4$. Since most of the times multiband photometry is used, the problem is ultimately reduced to a proper derivation of physical fluxes (erg s^{-1} cm^{-2} Å^{-1}) from magnitudes, i.e. to the underlying photometric absolute calibration.

Without exaggeration, this is the most critical point when implementing the IRFM, as already recognized in Blackwell et al. (1990). Casagrande et al. (2010) further highlighted how any difference between IRFM scales in the literature could be simply explained by changing the absolute calibration of the adopted photometric systems, or equivalently using different photometric zero-points. In this sense, changing filter sets and/or zero-points corresponds to introducing different IRFM scales. This also implies that homogeneous and well-standardized photometry must be used, and filter transformation from one system to the other preferentially avoided, since systematic zero-point offsets are often hidden in the scatter of different colour transformations. This was the main motivation to obtain and analyse in this work dedicated near-infrared photometry for our sample stars.

3.1 The IRFM in this work

We use the same IRFM implementation described in Casagrande et al. (2006, 2010, and references therein), where the relevant formalism on transforming heterochromatic measurements into monochromatic quantities at the corresponding star plus filter effective wavelength, taking into account energy or photocounting integration, can also be found. The bolometric flux is recovered using multiband optical and near-infrared photometry, and the flux outside of these bands is estimated using a theoretical model flux at a given T_{eff}, [Fe/H] and log g. The adopted [Fe/H] and log g for each star are reported in Table 1, while an iterative procedure is adopted to converge in T_{eff}. For internal consistency, we preferred gravity and metallicity data from Casagrande et al. (2011), or from spectroscopic studies adopting a T_{eff} scale consistent with theirs; but, the specific choice of [Fe/H], log g and model atmospheres typically affects the IRFM temperatures, separately, by $\sim$10 K at most, for the reasons explained above (see similar comparison e.g. in Alonso et al. 1996a).

The effect of random photometric errors on $\mathcal{F}_{bol}$, T_{eff} and θ for each star are derived using a Monte Carlo simulation and added in quadrature to the uncertainty stemming from a change of $\pm$0.5 dex in log g and $\pm$0.2 dex in metallicity. The error in metallicity includes a typical 0.1 dex precision of abundance determinations, and an additional systematic uncertainty by the same amount, corresponding to a possible shift of 100 K in the assumed T_{eff} – which is the accuracy we aim to test. (Note though that such metallicity–temperature interplay only refers to spectroscopic estimates; in the IRFM, a change of 0.1 dex in [Fe/H] affects the temperatures typically by less than 10 K.) Finally, we increased all errors by an additional 20 K in effective temperature, 1.0 per cent in $\mathcal{F}_{bol}$ and 0.7 per cent in θ, which are the zero-point uncertainties derived in Casagrande et al. (2010).

All of our sample stars have *Hipparcos* distances closer than 72 pc (van Leeuwen 2007) and are well within the local bubble, where reddening is negligible (e.g. Leroy 1993; Lallement et al. 2014). This is important for robust IRFM results, since a change of 0.01 mag in $E(B - V)$ would affect the T_{eff} at the level of 50 K (Casagrande et al. 2010).

In the following subsections, we present the results obtained implementing the IRFM in different photometric systems (i.e. with the filter transmission curves, zero-points and absolute fluxes appropriate to each), which effectively correspond to introducing (slightly) different IRFM scales. In the optical, we use the Tycho2 system, well standardized and homogeneous for magnitudes brighter than about 10 which is always the case in the present study. For a subset of stars, Johnson–Cousins photometry is also available and used; while it provides a more complete coverage of the optical part of a spectrum, in the T_{eff} range explored here, this choice is fortunately irrelevant (see Section 3.1.3). Also, until recently optical photometry of solar twins was available only in the Tycho2 system; this gap has now been amended, thanks to the observational efforts of Ramírez et al. (2012) and the solar calibration of the IRFM tested in both Tycho2 and Johnson–Cousins system (Casagrande et al. 2012). However, what really drives the derived stellar parameters in our technique is of course the infrared photometry, i.e. 2MASS *JHK$_s$* and SAAO *JHK* magnitudes. Since we ultimately aim to test the calibration of our IRFM scale in the widely used 2MASS system, the best approach is to adjust the SAAO absolute flux calibration to yield effective temperatures and diameters consistent with 2MASS. Within the IRFM, this is a far more robust way of tying the two systems together, rather than a star-by-star conversion of magnitudes. We discuss all these subtleties further below.

3.1.1 Tycho2–2MASS

The IRFM implementing the Tycho2 $B_T V_T$ (Høg et al. 2000) and 2MASS *JHK$_S$* (Cutri et al. 2003) photometric system takes advantage of the well-defined absolute calibration in the infrared (Cohen
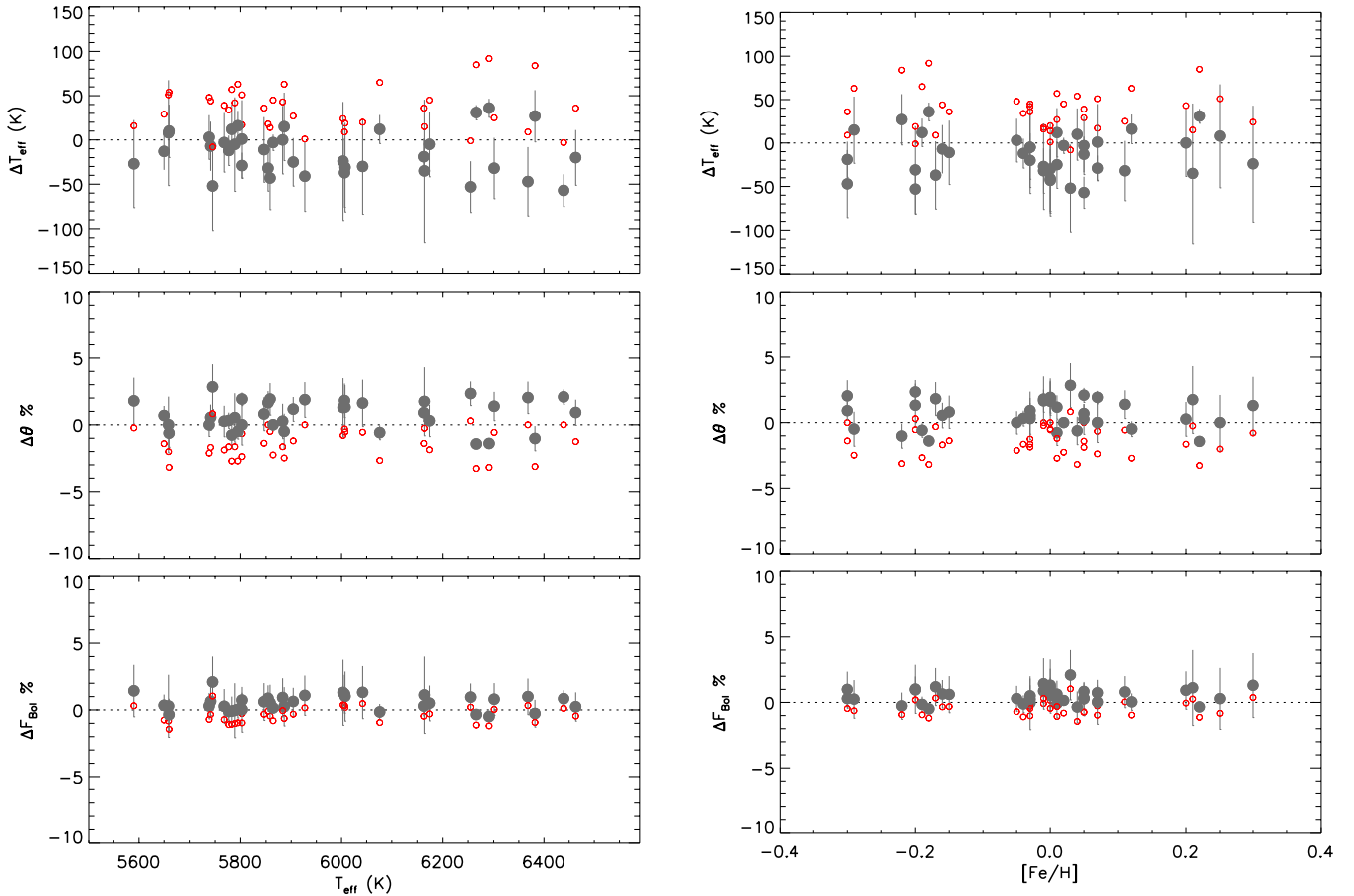
Figure 1. Comparison (SAAO minus 2MASS) of $T_{\rm eff}$, θ and $\mathcal{F}_{\rm bol}$ obtained implementing the two systems in the IRFM, for 38 stars in common. The open circles refer to the comparison before adjusting the SAAO absolute flux calibration and filled points after increasing it by 3 per cent.

et al. 2003; Rieke et al. 2008): its zero-point is calibrated with a claimed accuracy of $\sim$20 K using solar twins (Casagrande et al. 2010). 38 stars in Table 1 satisfy the 2MASS quality requirement for reliably applying the IRFM (i.e. 'j_'+'h_'+'k_msigcom' <0.15), all but one having photometric quality flag 'AAA'.[2]

3.1.2 Tycho2–SAAO

The SAAO *JHK* filter set has been implemented in our IRFM procedure. Observationally, the zero-points of the SAAO *JHK* photometric system are based on 25 early main-sequence stars (Carter 1990). Since Vega is unobservable in the Southern hemisphere, it cannot be used as primary flux calibrator, and Sirius is often chosen as a complementary or alternative standard (e.g. Cohen et al. 1992); Casagrande et al. (2008) derived the absolute calibration of the SAAO system by scaling a Kurucz synthetic spectrum of Sirius with the interferometric angular diameter measurement of Kervella et al. (2003b). However, resorting to this absolute calibration would introduce yet a slightly different $T_{\rm eff}$ scale from the 2MASS-based one we wish to test.

Therefore, we opt to let the SAAO *JHK* absolute calibration vary, until the resulting weighted averages of $T_{\rm eff}$, θ and $\mathcal{F}_{\rm bol}$ derived from Tycho2–SAAO photometry agree with those from Tycho2–2MASS for 38 stars in common (Fig. 1). Apart from

[2] http://www.ipac.caltech.edu/2mass/releases/allsky/doc/sec2_2a.html

the infrared photometry, all other input parameters are the same ($B_T V_T$, [Fe/H] and $\log g$); thus, in the weighted average, only the internal accuracy is considered, and this can be immediately estimated from the scatter returned from each infrared band used in the IRFM. With a 3 per cent increase in the SAAO absolute flux calibration of Casagrande et al. (2008), we achieve an agreement with the Tycho2–2MASS-based scale of $\Delta T_{\rm eff} = -1 \pm 4$ K ($\sigma = 24$ K), $\Delta\theta = -0.01 \pm 0.11$ per cent ($\sigma = 1.10$ per cent) and $\Delta\mathcal{F}_{\rm bol} = +0.1 \pm 0.1$ per cent ($\sigma = 0.6$ per cent). The 3 per cent adjustment in absolute calibration is relatively minor, and still in accordance with the 2 per cent uncertainty estimated in Casagrande et al. (2008, we recall here that the best absolute flux scale currently available from the *HST* is at the per cent level; see Bohlin 2007); without this, SAAO-based IRFM temperatures would be systematically hotter by about 30 K.

3.1.3 Johnson–Cousins–SAAO

A subset of 25 stars also has Johnson–Cousins $BV(RI)_C$ photometry from the literature (Table 1); this allows us to implement the IRFM using this system, for further comparison. Although $BV(RI)_C$ photometry provides a more complete coverage of the spectral energy distribution, Casagrande et al. (2010) verified that there is essentially no difference with respect to using only $B_T V_T$ Tycho2 (at least for temperatures >5000 K), the near-infrared calibration still being the dominant ingredient.

Table 2. IRFM $T_{\rm eff}$ for solar twins. In both cases, errors do not include the zero-point uncertainty in the effective temperature scale (see Casagrande et al. 2010).

HD	HIP	Tycho2–SAAO $T_{\rm eff}$	Tycho2–2MASS $T_{\rm eff}$	JC–SAAO $T_{\rm eff}$
71334	41317	5741 ± 22	5739 ± 27	5719 ± 32
78534	44935	5774 ± 29	5803 ± 30	5790 ± 36
78660	44997	5784 ± 25	5791 ± 30	5726 ± 30
115169	64713	5822 ± 36	5853 ± 36	5740 ± 32
142331	77883	5670 ± 30	5660 ± 35	5674 ± 33
167060	89650	5861 ± 29	5864 ± 35	5823 ± 34
146233	79672	5819 ± 26		5789 ± 38
138573	76114	5765 ± 23	5777 ± 25	
Weighted mean		5778 ± 20	5782 ± 25	5750 ± 19

For stars in common, the difference in the IRFM (Johnson–Cousins–SAAO minus Tycho2–SAAO) is $\Delta T_{\rm eff} = -25 \pm 6$ K ($\sigma = 31$ K), $\Delta\theta = 0.3 \pm 0.1$ per cent ($\sigma = 0.4$) and $\Delta\mathcal{F}_{\rm bol} = -1.0 \pm 0.2$ per cent ($\sigma = 1.2$), i.e. the IRFM in the Johnson–Cousins–SAAO system returns slightly cooler temperatures, lower bolometric fluxes and larger angular diameters. A similar -25 K offset was found by Casagrande et al. (2012) using Johnson–Cousins–2MASS versus Tycho2–2MASS photometry.

From the SAAO over 2MASS calibration in the previous section, and the Tycho2 versus Johnson comparison carried out here, we can conclude that changing the adopted filter set can systematically affect temperatures by $20-30$ K, in agreement with the zero-point uncertainty of 20 K estimated by Casagrande et al. (2010) and is included in our global error estimate.

3.2 Solar twins

The zero-point of the Tycho2–2MASS (and Johnson–Cousins–2MASS) scale of Casagrande et al. (2010) was finely tuned to render the solar temperature on average for a set of 10 spectroscopically selected solar twins. These were identified with a purely differential analysis with respect to a solar reference spectrum, obtained with the same instrument and observing run, without assuming a priori any $T_{\rm eff}$ (Meléndez & Ramírez 2007; Meléndez et al. 2009; Ramírez et al. 2009), so that they truly serve as an independent test of the temperature scale.

Six of them have SAAO near-infrared photometry from this work; the corresponding IRFM temperatures are listed in Table 2. We also include the solar twins 18 Sco (Porto de Mello & da Silva 1997; Bazot et al. 2011) and HD138573 (Datson et al. 2012). The Tycho2–2MASS and Tycho2–SAAO systems are clearly well calibrated with each other, with typical differences of only a few kelvin (median 7 ± 6 K, $\sigma = 15$ K). The absolute solar calibration of our IRFM is also confirmed, as the average effective temperature is very close to $T_{\rm eff,\odot}$ for the Tycho2–2MASS and Tycho2–SAAO cases (while the Johnson–SAAO estimate is cooler by about 25 K, in agreement with Section 3.1.3).

4 TESTING THE ZERO-POINT VERSUS INTERFEROMETRY

The main purpose of this work is to compare angular diameters derived from the IRFM to interferometric measurements, so as to check the IRFM diameter (and thus temperature) scale. While such a test is certainly fundamental, we warn that the calibration of the interferometric scale is not straightforward to assess: comparisons between diameters obtained from PTI and CHARA suggest possible systematics at the 6 ± 6 per cent level (van Belle & von Braun 2009; Boyajian et al. 2012a), corresponding to about 150 K in temperature; and systematics appear even when the same interferometer but different beam combiners are used (e.g. Boyajian et al. 2012b; White et al. 2013). Although the evidence is as yet poorly quantified, it is very important if we aim at setting the zero-point of the $T_{\rm eff}$ scale to better than 1 per cent (i.e. about 2 per cent in angular diameters). Also, the correction from uniform disc measurement to limb-darkened diameter plays a role. In particular, 3D model atmospheres provide a more realistic description of the centre-to-limb variation (Pereira et al. 2013), and the resulting limb-darkening coefficients imply angular diameters smaller by $0.5-1.0$ per cent, the exact value depending on the parameters of the star analysed, as well as on the wavelength of observation (e.g. Allende Prieto et al. 2002; Aufdenberg, Ludwig & Kervella 2005; Bigot et al. 2006; Chiavassa et al. 2010, 2012). All the stars used in this paper have interferometric limb-darkened diameters computed using 1D models (with the exception of HD122653 discussed below in Section 4.3), and likely to be overestimated by the amount mentioned above.

4.1 Comparing angular diameters

The fundamental comparison with interferometry relies on angular diameters (directly measured) rather than on effective temperatures, which are secondary quantities obtained by combining the above measurements with a reconstruction of bolometric fluxes. From our sample of stars having SAAO infrared photometry, we searched recent literature looking for interferometric measurements (first part of Table 3; additional stars in the same table with unsaturared 2MASS photometry are discussed later).

Cherry-picking single measurements from the literature would introduce a degree of freedom difficult to assess, and indeed we verified that with 'appropriate' choices in the data set to consider, the offsets discussed later can essentially reduce to zero. To avoid such a bias, we assemble a blind sample: for stars having multiple measurements we computed their weighted average with weights $w_i = 1/\sigma_i^2$, where σ_i is the quoted uncertainty of each measure. Multiple measurements allow us to estimate realistic error bars via the weighted sample variance $\frac{\sum_i w_i(x_i-\mu)^2}{\sum_i w_i}$, which essentially measures the overdispersion of the data with respect to the simple variance of the weighted mean $1/\sum_i w_i$. This simple exercise suggests that – for the sample available here – realistic interferometric error bars for measurements below 1 mas should be $\gtrsim 0.01$ mas.

In contrast, the accuracy of the angular diameters determined via IRFM stays constant at the $1-2$ per cent level independently of the size of the star. This means that the best regime for testing the $T_{\rm eff}$ scale is by using stars with diameters of the order of $\gtrsim 1$ mas. One should not disregard, however, the most recent measurements with spectacular sampling of visibilities achieving indeed robust submilliarcsec results (White et al. 2013).

Fig. 2 shows the difference between IRFM and interferometric angular diameters, as a function of temperature, diameter, metallicity and gravity. No significant trend is detected and the offsets are of a pure zero-point nature, as appropriate for the IRFM. From the bottom-left panel, it is clear that the comparison is most meaningful at $\theta \gtrsim 0.8-0.9$ mas; scatter and uncertainties significantly increase when including data with smaller diameters. This is highlighted in the top panel of Fig. 3, where the weighted mean difference (and corresponding scatter) between the IRFM and interferometric

Table 3. Angular diameters and effective temperatures measured from interferometry and obtained from the IRFM in different systems. The first 16 stars are from our SAAO sample, while the remaining are in the 2MASS system (see discussion in the text).

HD	θ	Ref.	Tycho2–SAAO $T_{\rm eff}$	θ	JC–SAAO $T_{\rm eff}$	θ	Tycho2–2MASS $T_{\rm eff}$	θ
30652	1.525 ± 0.010	1,2	6536 ± 59	1.511 ± 0.021	6493 ± 62	1.519 ± 0.021	–	–
39587	1.053 ± 0.011	1,2	5972 ± 40	1.053 ± 0.013	–	–	–	–
48737	1.401 ± 0.009	2	6553 ± 60	1.381 ± 0.018	–	–	–	–
56537	0.835 ± 0.013	2	8346 ± 136	0.770 ± 0.016	–	–	–	–
75732	0.711 ± 0.004	3	5295 ± 36	0.689 ± 0.008	–	–	–	–
97603	1.324 ± 0.021	1,2	8115 ± 123	1.298 ± 0.025	–	–	–	–
102870	1.433 ± 0.006	2,4	6146 ± 45	1.419 ± 0.016	6118 ± 56	1.423 ± 0.017	–	–
118098	0.852 ± 0.009	2	8240 ± 129	0.858 ± 0.018	8154 ± 118	0.863 ± 0.018	–	–
131977	1.177 ± 0.030	5	4614 ± 40	1.156 ± 0.016	4614 ± 38	1.157 ± 0.013	–	–
141795	0.768 ± 0.017	2	8287 ± 129	0.729 ± 0.014	8203 ± 117	0.732 ± 0.013	–	–
142860	1.217 ± 0.005	1,2	6345 ± 56	1.197 ± 0.018	–	–	–	–
146233	0.676 ± 0.006	6	5819 ± 41	0.671 ± 0.010	5789 ± 53	0.674 ± 0.010	–	–
164259	0.775 ± 0.027	2	6809 ± 74	0.713 ± 0.011	6777 ± 75	0.716 ± 0.011	–	–
173667	1.000 ± 0.006	2	6425 ± 58	0.980 ± 0.014	–	–	–	–
177724	0.895 ± 0.017	2	9152 ± 122	0.888 ± 0.014	–	–	–	–
182572	0.845 ± 0.025	2	5550 ± 36	0.870 ± 0.009	5537 ± 46	0.871 ± 0.010	–	–
173701	0.332 ± 0.006	7	–	–	–	–	5357 ± 91	0.324 ± 0.013
175726	0.346 ± 0.007	7	–	–	–	–	6079 ± 120	0.346 ± 0.016
(g)175955	0.680 ± 0.010	7	–	–	–	–	4766 ± 97	0.656 ± 0.032
(g)177151	0.570 ± 0.010	7	–	–	–	–	5016 ± 84	0.535 ± 0.021
177153	0.289 ± 0.006	7	–	–	–	–	6063 ± 115	0.279 ± 0.012
†181420	0.340 ± 0.010	7	–	–	–	–	6637 ± 129	0.307 ± 0.014
(g)181827	0.473 ± 0.005	7	–	–	–	–	4997 ± 92	0.490 ± 0.022
182736	0.436 ± 0.005	7	–	–	–	–	5205 ± 98	0.443 ± 0.020
187637	0.231 ± 0.006	7	–	–	–	–	6290 ± 115	0.223 ± 0.010
(g)189349	0.420 ± 0.006	7	–	–	–	–	5000 ± 89	0.441 ± 0.018
					Johnson–Cousins–2MASS			
122563	0.940 ± 0.011	8	–	–	4600 ± 47	0.941 ± 0.019	–	–

Notes. Source of interferometric measurement. In case of multiple entries, weighted average is taken (see the text for details). 1– van Belle & von Braun (2009); 2– Boyajian et al. (2012a); 3– von Braun et al. (2011); 4– North et al. (2009); 5– Demory et al. (2009); 6– Bazot et al. (2011); 7– Huber et al. (2012), with prefix (g) for giants; 8– Creevey et al. (2012). †Interferometric measurement to be regarded with suspicion due to problem with the calibrator (Huber, private communication).

results is plotted as a function of the threshold above which angular diameters are considered: $\theta_{\rm min}$. The $\theta_{\rm min}$ diagram (TM-diagram) first introduced here is a handy graphic diagnostic to assess whether a given interferometric data set is affected by systematic trends. In fact, while the smaller the diameter the more challenging interferometric measurements are, a photometric technique like the IRFM is insensitive to that. The plot also visualizes how stable the comparison is, when relying on just a few high-quality data points (right-hand side of the plot) or a larger data set including smaller and less-precise measurements. We will use this test again in Section 5.

We queried the SIMBAD data base to flag possible troublesome stars; HD56537 and HD173667 include two components (thus affecting their photometry), while HD118098 has a faint stellar companion. In the latter case, the difference in H band is 7 mag (Hinkley et al. 2010), so the contribution to the flux can be readily computed to be of the order of 0.1 per cent, i.e. 10 times smaller than observational uncertainties. In the cases of HD56537 and HD173667, we carried out the comparison with and without these two stars: for the culled sample, the offsets are slightly reduced, but the change is marginal so, for simplicity, we report only the results of the full sample. Similarly, our IRFM sample reflects the status of a rapidly evolving literature, and it does not include any of the robust submilliarcsec measurements of White et al. (2013, their 16 Cyg B having good 2MASS photometry), while we learnt that the interferometric measurement of HD181420 should be disregarded due to problems

with the calibrator (Huber, private communication). Both updates would improve the agreement between the IRFM and interferometry, but in the spirit of a blind sample, we refrain from playing any minor star-in/star-out game with the sample. Also, we find very similar offsets when using other statistical estimators (simple mean or median, rather than weighted mean).

All in all, in the regime most relevant for the comparison ($\theta \gtrsim 0.8$–0.9 mas), we find offsets in diameters of the order of -1.0 per cent for the Tycho2–SAAO IRFM stars and -0.5 per cent for the Johnson–Cousins–SAAO IRFM stars. This is consistent with the average offset of -0.62 ± 1.7 per cent found in Casagrande et al. (2010) applying $T_{\rm eff}$ and bolometric flux calibrations to an almost entirely different set of stars.[3] Thus, the comparisons performed in that work were sound, albeit indirect.

The above offsets in angular diameters translate into $T_{\rm eff}$ hotter by ~ 0.5 and 0.25 per cent, i.e. by $\sim +30$ and $\sim +15$ K at the solar value. We conclude that, depending on the exact filter set used, the IRFM scale agrees with interferometry on average within about 20 K, as originally claimed. Such offset is comparable to the systematic change expected when adopting 3D limb-darkening

[3] Only three of the stars in the present sample overlap with those used in Casagrande et al. (2010, cf. their table 3): HD75732, HD102870 and HD131977, all in excellent agreement within errors.
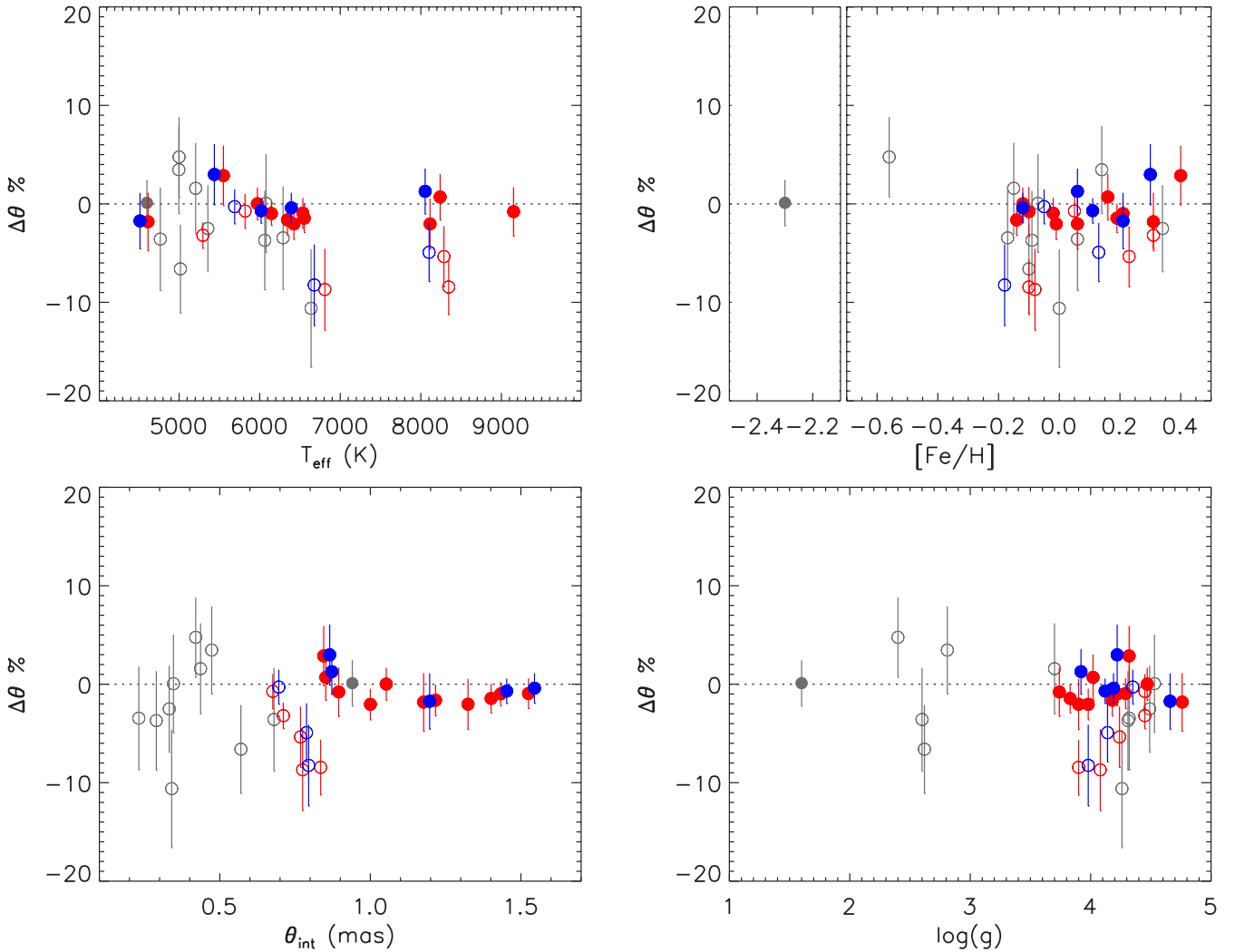
Figure 2. Difference between interferometric angular diameters and those derived via the IRFM ($\Delta\theta = 1 - \theta_{int}/\theta_{IRFM}$ in per cent). The filled symbols are for stars with interferometric diameters greater than 0.84 mas (threshold above which the scatter with respect to interferometry is minimized, cf. Fig. 3 and discussion in the text). The colours refer to the photometric systems implemented in the IRFM: Tycho2–SAAO in red, Johnson–Cousins–SAAO in blue (abscissa values slightly shifted for clarity). Grey open circles are for stars from Huber et al. (2012) and the filled grey dot is for HD122563.

corrections in interferometric measurements (e.g. Allende Prieto et al. 2002; Chiavassa et al. 2010), possibly bringing the two scales in even closer agreement. Considering the systematics involved in interferometric measurements (see also Section 5), one may actually argue that the reliability of the latest absolute fluxes (at the per cent level; Bohlin 2007) and the solar twin calibration rival interferometry in setting the temperature scale. The offsets we find are in fact at a level where also interferometric measurements are plagued by systematics.

4.2 Comparing temperatures

The comparison in terms of directly measured angular diameters is the most robust; comparison to interferometric temperatures is less straightforward, for these involve an additional reconstruction of the bolometric flux. As the flux derivation is independent in the two approaches, the comparison between temperatures may introduce additional noise and systematics. In particular, interferometric papers often allow reddening as a free parameter in the fit of the spectral energy distribution (e.g. van Belle & von Braun 2009;

Boyajian et al. 2012a), while for stars as nearby as those in our sample, an assumption of negligible reddening is more appropriate.

Nonetheless, as it is customary for the various temperature scales in the literature to be compared to interferometric T_{eff}'s, in the bottom panel of Fig. 3, we also perform this check for the stars in Table 3 where literature reports interferometric temperatures along with diameters (the majority). Reassuringly, the resulting temperature offsets are consistent with the more direct comparison of diameters in the previous section: the independent reconstruction of $\mathcal{F}_{bol}$ in the two methods does not result in any significant systematic differences.

4.3 Giants and the benchmark metal-poor case: HD122563

The increasing capabilities of interferometers are pushing the limit to which angular diameters can now be measured, in particular using optical beam combiners. Recently, Huber et al. (2012) measured angular diameters <0.7 mas for a number of stars with unsaturated 2MASS photometry; these stars are listed in the second part of Table 3 and included in Figs 2 (grey open circles) and 3 (grey lines).
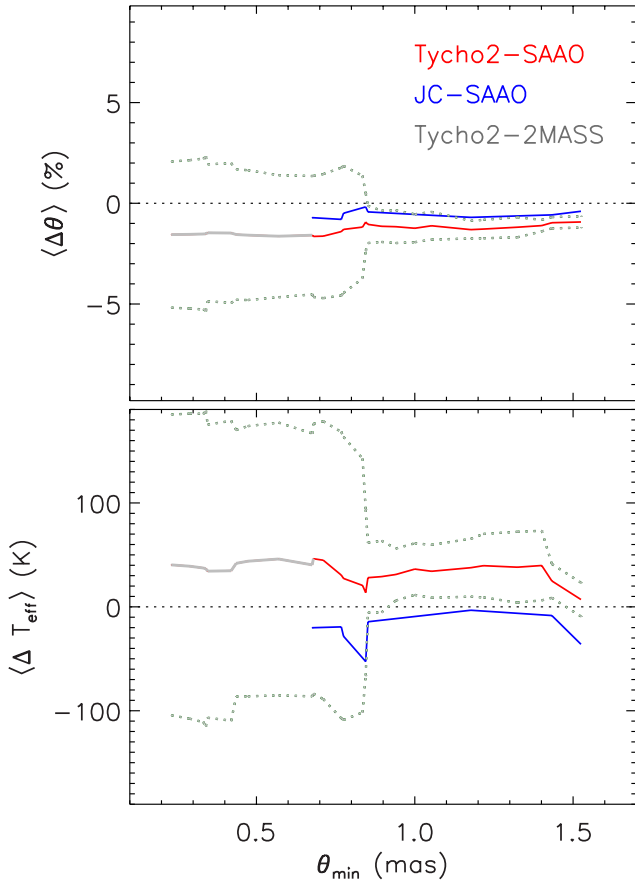
Figure 3. TM-diagram. Top panel: weighted mean difference (in per cent) between angular diameters from interferometry and the IRFM as a function of the threshold above which interferometric diameters are considered ($\theta_{\min}$). The dotted lines are for 1σ error bars scatter for the Tycho2–SAAO/2MASS comparison. Bottom panel: same as above, but for weighted mean difference in effective temperatures $\langle \Delta T_{\rm eff} \rangle$.

Their main conclusion is that angular diameters from interferometry and the IRFM agree within -2 ± 2 per cent ($\sigma = 5$ per cent); or -1.4 ± 1.5 per cent in weighted average. This agrees with what we found in the previous section for our SAAO stars with larger and more accurate diameters. More interestingly, four stars in Huber et al. (2012) are giants; their diameters agree very well with our estimates: 0.0 ± 2.3 per cent ($\sigma = 5.5$ per cent) in weighted average.

Because of its relevance as a standard metal-poor star, we include in the discussion also HD122563 for which the angular diameter has been recently measured, and corrected using 3D limb-darkening coefficients (Creevey et al. 2012). As there is no SAAO *JHK* photometry for this star and its 2MASS data are saturated, for this one star we resort to filter transformations from Johnson *JHK* to 2MASS using the updated Carpenter (2001) transformations; Johnson–Cousins photometry is used in the optical. The star is a giant located at $\sim$240 pc (van Leeuwen 2007) and reddening must be considered. We adopt $A_v = 0.01$ from Creevey et al. (2012), which corresponds to $E(B - V) = 0.003$, in very close agreement with estimations from interstellar NaD lines in high-resolution spectra of this star (Bergemann, private communication). Thus, reddening has a minor contribution to the global error budget, $T_{\rm eff}$ being only 8 K cooler should attenuation be zero. This metal-poor star is displayed in Fig. 2 as a filled grey dot: the agreement between IRFM and interferometric results is near perfect. Together with a former test using

HST absolute spectrophotometry (Casagrande et al. 2010), this result confirms the robustness of the IRFM also at low metallicities. Setting the $T_{\rm eff}$ scale in the metal-poor regime is crucial, since an uncertainty of 100 K can rival with NLTE effects on determinations of iron abundance (Ruchti et al. 2013), and affect the lithium level on the Spite plateau, with cosmological implications (e.g. Meléndez et al. 2010a; Sbordone et al. 2010; Nordlander et al. 2012).

5 THE INTERFEROMETRIC SCALE: A CAUTIONARY TALE

One of the original motivations behind this work was to test the temperature scale of the Geneva–Copenhagen Survey. The latest official rendition (GCSIII; Holmberg et al. 2009)[4] and the independent analysis of the same sample based on the IRFM scale differ by about 80 K (Casagrande et al. 2011, hereafter C11, being hotter), yet both authors claim agreement with interferometry within the errors. It was pointed out that considering a dozen stars in common between the Geneva–Copenhagen catalogue and the recent CHARA data set of Boyajian et al. (2012a) with $\theta \geq 1$ mas, GCSIII temperatures are on average in excellent agreement with the interferometric scale, while C11 temperatures are too hot by about 70 K – at odds with our results so far. Even more confusingly, Boyajian et al. (2012a) reported good agreement with the $(B - V)$ colour–metallicity–$T_{\rm eff}$ relation of Casagrande et al. (2010), but found GCSIII temperatures to be too *hot* by 100 K or more.

Spurred by this, we applied the TM-diagram to the data set of Boyajian et al. (2012a), which has 25 stars in common with either GCSIII or C11.[5] Note that all stars discussed in the remaining of this section have effective temperatures derived from the Strömgren $(b - y)$ index, if not otherwise specified. This is the colour used in GCSIII for all targets and in C11 for stars with unreliable 2MASS photometry to apply the IRFM (indeed the case for all nearby interferometric targets).

In Fig. 4 (top panel), we show the effective temperature difference between the two Strömgen scales and the Boyajian et al. (2012a) data set, plotted as a function of interferometric angular diameters. A clear trend appears, which is further highlighted in the bottom panel with the TM-diagram, where the average difference with respect to the above interferometric temperatures $\langle \Delta T_{\rm eff} \rangle$ is shown for various thresholds in angular diameters. While the constant difference between GCSIII and C11 reflects the zero-point difference of these two photometric scales (and their similar internal consistency), the trend with respect to the interferometric measurements of Boyajian et al. (2012a) suggests the presence of systematic effects in the latter sample. We also verified that our conclusions still hold should this plot be made with $T_{\rm eff}$ derived from colour indices other than Strömgren (the value of the offset using other colours might vary by a few tens of K – compatible with the intrinsic difference when using different indices on a rather limited number of stars – but the trend remains).

This systematic trend hampers robust conclusions on the $T_{\rm eff}$ zero-points from this data set: the offset between GCSIII and Boyajian

---

[4] For convenience in the following, we refer to GCSIII, although stellar parameters were derived in GCSII; see discussion in section 2.1.1 of Casagrande et al. (2011).

[5] From an initial sample of 33 stars in common, we exclude seven objects for which photometry includes more than one component, as marked by the corresponding label (usually 'AB'). As recommended in C11, users are warned against their use, although we verified that the overall conclusions still hold, should these stars be kept.
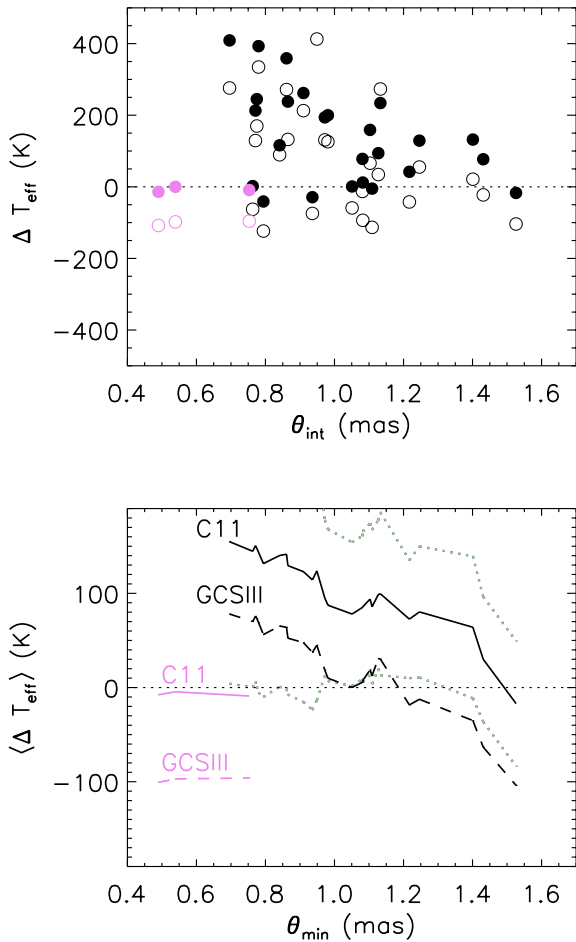
in White et al. (2013), Ligi et al. (2012) independently confirm a diameter significantly smaller, and thus a hotter T_{eff}, than Boyajian et al. (2012a). Considering the stars of White et al. (2013) in Fig. 4 shows no trends with diameter, as one would expect, and yields good agreement of C11 with this particular interferometric set.

In retrospective, we stress that no trend is present in Fig. 3, based on a compilation from literature (including Boyajian et al. 2012a, refraining from its exclusion in the spirit of a blind sample), but averaging over multiple measurements of the same star when available. We also remark that in Fig. 3 the scatter at all θ_{min} is also much lower than in Fig. 4, and excluding the data set of Boyajian et al. (2012a) from Table 3 does not change significantly the conclusions of Section 4.

The suspicion that there are systematic trends in the Boyajian et al. (2012a) data set is further highlighted once the same comparison is performed with respect to other measurements in literature (see the caption of Fig. 5). Over a wide range of angular diameters, this comparison shows a rather constant offset in effective temperature (left-hand panel in Fig. 5). It also confirms the known offset of about 80 K between GCSIII and C11, and it shows how the two scales are compatible with interferometry within ± 50 K or better, on the cool and hot side, respectively. This is not entirely surprising, now: the effective temperatures used for this comparison are in fact all derived from the $(b - y)$ colour. This Strömgren index was calibrated against T_{eff} derived in a more direct way (the 'parent scales'): the IRFM in C11 and the di Benedetto (1998) surface-brightness relation in GCSIII. We verified from over 70 common stars that the parent scales differ by about 40 K. Consistently with the offsets found in Section 4 for the IRFM, the di Benedetto (1998) scale is in good agreement with interferometry, but on the cooler side (-9 ± 22, $\sigma = 108$ K, for 25 of his stars with modern interferometric data). Thus, the same must be true for effective temperatures derived from their colour calibrations, but with important caveats. We verified that *on average* the effective temperatures derived from the $(b - y)$ index are both excellent renditions of the corresponding parent scales; although when considering a limited number of stars, zero-point differences of a few tens of kelvin are possible (cf. also Muñoz Bermejo, Asensio Ramos & Allende Prieto 2013). These differences stem both from the fact that the colour relations are not always a perfect rendition of the calibrating sample over the full parameter space, as well as from the photometric errors associated with measurements in each colour index. In particular, the sensitivity of $(b - y)$ to metallicity as well as its steep correlation with T_{eff} make this colour index less than optimal for discriminating the zero-point of various effective temperature scales: a change of only 0.010–0.015 mag in $(b - y)$ corresponds to a shift of 100 K, a change which can be as small as 0.007 mag if the joint effect of metallicity is included. Thus, it is not surprising that in Fig. 5 the $(b - y)$ effective temperatures of both GCSIII and C11 have a somewhat different offset than expected from the parent scales (di Benedetto or the direct IRFM comparison of Section 4).

Our tests show that the offsets derived for colour-calibrated temperature scales are quite sensitive to the specific subsample of interferometric stars considered for comparison, and we illustrate this with a Monte Carlo simulation in the right-hand panel of Fig. 5. To this purpose, we have run 2×10^6 different realization of the sample used in the left-hand panel. For each realization we took a subsample random in number of entries. The plot shows the distribution of the median and mean weighted average difference of GCSIII and C11 with respect to these random interferometric subsamples. Depending on the subsample considered, somewhat different zero-point values are inferred from such a comparison. This together
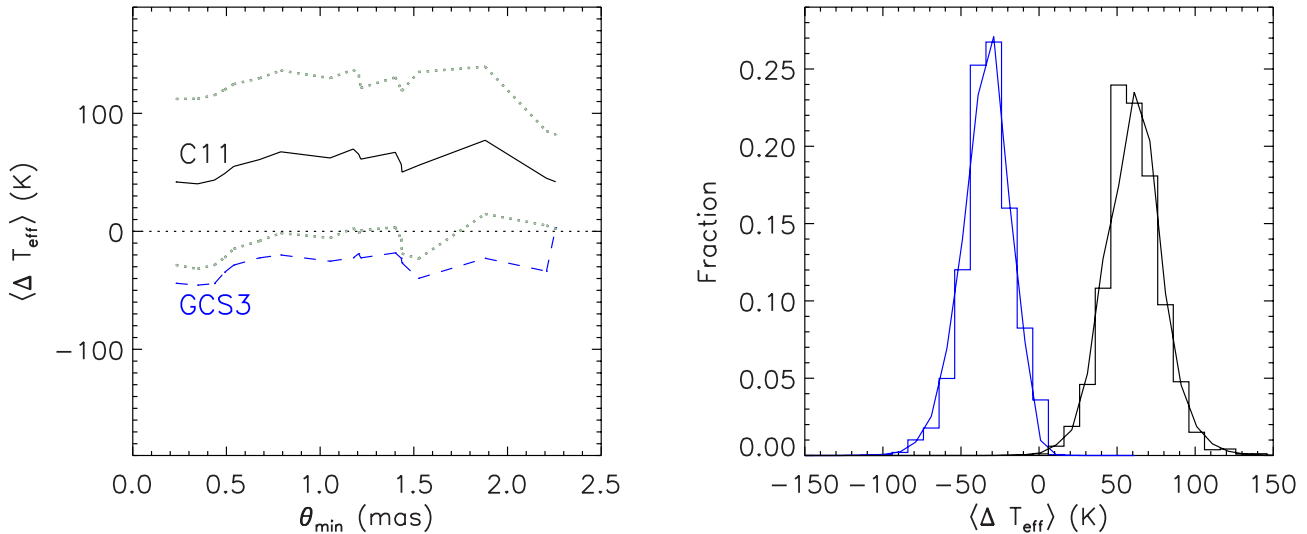
Figure 4. Top panel: effective temperatures of Casagrande et al. (2011, filled circles) and Holmberg et al. (2009, open circles) with respect to interferometric measurements of Boyajian et al. (2012a, black) and White et al. (2013, purple). Bottom panel: weighted mean difference for stars in the top panel as a function of the threshold above which interferometric angular diameters are considered (TM-diagram). 1σ errors with respect to C11 are included for comparison (grey dotted lines).

et al. (2012a) is null if restricting to $\theta_{min} \geq 1$ mas, while when all common stars are considered, GCSIII is about 100 K hotter. This was indeed the claim in Boyajian et al. (2012a), and it would consequently imply that the C11 scale is too hot by about 200 K, which would be very surprising in view of the results in Section 4 for our SAAO sample, and the solar twins' test. We note further that the results of Boyajian et al. (2012a) for the famous solar twin 18 Sco (for which they obtain $\theta = 0.780 \pm 0.017$ mas, implying $R = 1.166 \pm 0.026$ $R_\odot$ and $T_{eff} = 5433 \pm 69$ K) fits the systematic trend highlighted in Fig. 4; while Bazot et al. (2011) with PAVO measure $\theta = 0.676 \pm 0.0062$ mas and confirm the strictly solar radius ($R = 1.010 \pm 0.009$ $R_\odot$), mass and T_{eff} of this star.

It is clearly hard to objectively set a threshold above which the comparison can be considered meaningful, and other interferometric measurements are required to gauge this problem. White et al. (2013) highlight underestimated errors and systematic offsets in the sample of Boyajian et al. (2012a). Both studies are carried out with CHARA, but the latter uses the PAVO optical beam combiner instead of Classic. PAVO allows us to probe the visibility curve at higher spatial frequencies, which are needed to derive robust angular diameters (see fig. 3 in White et al. 2013). For one of the targets

Figure 5. Left-hand panel: TM-diagram for effective temperatures in GCSIII and C11 from Table 3 plus interferometric measurements other than Boyajian et al. (2012a). Additional interferometric sources used are Mozurkewich et al. (2003), van Belle, Ciardi & Boden (2007), North et al. (2007), Kervella et al. (2008), van Belle & von Braun (2009), Demory et al. (2009), Huber et al. (2012), White et al. (2013). Only unreddened stars and with interferometric errors smaller than 5 per cent are used. Multiple measurements of same stars are averaged together as in Section 4. Right-hand panel: median (histogram) and mean (continuous line) distribution of the weighted effective temperature difference for 2×10^6 random realizations of the plot in the left-hand panel.

with the lower accuracy introduced when working with $T_{\rm eff}$ derived from colour relations explain why both GCSIII and C11 are still compatible with interferometry, while differing between them by as much as 80 K.

Since the two scales tie in this comparison, we shall comment on the scope of the adopted effective temperatures in GCSIII and C11, i.e. to determine stellar ages. To this purpose, in GCSIII the cooler effective temperatures were compensated by shifting the temperatures of the reference stellar isochrones, effectively erasing the difference between the two empirical scales. The hotter $T_{\rm eff}$ scale adopted in C11 also inspired a revision of the metallicity calibration, selecting spectroscopic measurements with temperatures consistent with the IRFM. We notice that 15 stars from the spectroscopic sources selected to calibrate metallicities in C11 can be now directly compared to *interferometric* temperatures from Fig. 5, showing good agreement for the adopted spectroscopic scale $\Delta T_{\rm eff} = -2 \pm 25$ K ($\sigma = 92$ K).

6 CONSTRAINING $T_{\rm eff}$ WITH PARALLAXES

Recently, asteroseismology has provided an alternative method to determine stellar masses and radii via scaling relations (e.g. Hekker et al. 2009; Stello et al. 2009; Silva Aguirre et al. 2011); the latter depend only loosely on the adopted $T_{\rm eff}$, and combination of asteroseismic radii with reliable angular diameter measurements can in principle yield *Hipparcos*-quality distances (Silva Aguirre et al. 2012).

While recent literature has focused on testing the scaling relations, there is by now a body of evidence suggesting that the latter are robust for main-sequence and subgiant stars (e.g. Chaplin & Miglio 2013, and references therein), so that we dare turn the argument around and use distances (parallaxes) to test the angular diameter and $T_{\rm eff}$ scale. This is still limited to a handful of stars, but here we propose the method with a view to application to future *Gaia* targets.

In Fig. 6, we compare *Hipparcos* distances to seismic ones, obtained by combining our (Tycho–2MASS) IRFM temperatures and

angular diameters with asteroseismic radii. The latter are computed as described in Silva Aguirre et al. (2012); the only improvement with respect to the values published there being the use of updated asteroseismic parameters (Chaplin et al. 2014) – although the effect is negligible on the scale of Fig. 6 and we verified that the same conclusions hold, should the previous set of frequencies be used.

As we have already extensively discussed, changing the near-infrared absolute calibration adopted in the IRFM returns different $T_{\rm eff}$, bolometric fluxes and angular diameters. Here, we explore the effect of changing the 2MASS absolute calibration by ± 5 per cent, which implies a change of about ∓ 100 K in effective temperatures and ± 3 per cent in angular diameters. It can be immediately appreciated that both a hotter or a cooler effective temperature scale return worse agreement in comparison with *Hipparcos*. What can be robustly concluded is that the method implemented in Silva Aguirre et al. (2012) is the one providing better distances, an important validation for using this technique in studies of Galactic structure.

7 CONCLUSIONS AND FUTURE PERSPECTIVES

In this paper, we performed a test of the IRFM temperature scale by Casagrande et al. (2010) versus the fundamental interferometric scale. Direct comparison between the two scales has been hindered by the lack of accurate, homogeneous near-infrared photometry for the nearby stars probed by interferometry. In particular, 2MASS photometry which is the basis for modern IRFM implementations is saturated for these nearby stars.

The purpose of this work was to fill this gap. We present dedicated SAAO *JHK* photometry for 55 stars, which allows us to directly implement the IRFM procedure on 16 nearby stars with measured angular diameters. The remainder of the sample has both SAAO and excellent 2MASS photometry and by acting only on the absolute calibration is used to secure that the present SAAO-based scale matches the 2MASS-based one of Casagrande et al. (2010). Note that to achieve the highest accuracy possible, no transformation between the two systems has been performed, rather the IRFM has
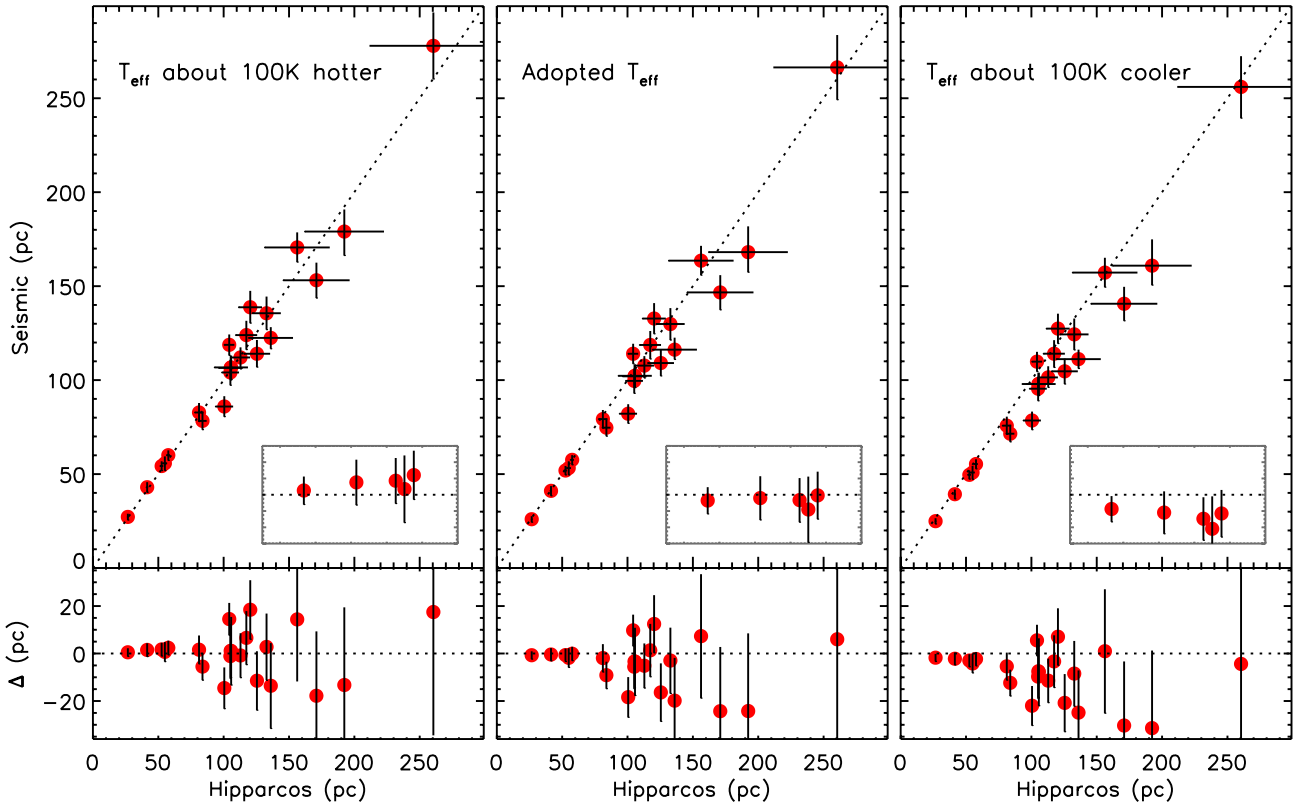
Figure 6. Seismic distances of main-sequence and subgiant stars relying on our T_{eff} and angular diameter scale compared to *Hipparcos* distances. The effect of changing the infrared absolute calibration and thus the T_{eff} scale by roughly ± 100 K is shown on the left- and right-hand panels. Beyond 60 pc, uncertainties largely increase due to reddening. Insets in the top panels zoom on to stars closer than 70 pc where reddening is not an issue.

been implemented for each system using the most reliable absolute calibration, zero-point and filter transmission curves. When this is done, the specific choice of filter set (optical: Johnson–Cousins versus Tycho2 or near-infrared: SAAO versus 2MASS) affects the IRFM temperatures by about $20-30$ K.

Comparison to interferometric data with the best direct measurements ($\theta \gtrsim 0.8-0.9$ mas) reveals offsets between 0.5 and 1.0 per cent in angular diameter (the IRFM scale having smaller diameters and thus hotter T_{eff}, by $15-30$ K), depending on the exact filter system in use. These offsets are close to those indirectly derived in Casagrande et al. (2010) using colour calibrations, thus confirming the results of that analysis. Considering that essentially all interferometric diameters considered here have limb-darkening corrections computed from 1D model atmospheres, adoption of more realistic 3D corrections is deemed to largely remove the above-mentioned difference, bringing the direct and IRFM scale into even closer agreement. Indeed, in a future work, we intend to revise interferometric measurements using limb-darkening corrections computed from the 3D hydrodynamical stellar atmosphere models with the STAGGER code by Magic et al. (2013).

The IRFM temperature scale in this work is confirmed to be well calibrated on solar twins, as was the original scale of Casagrande et al. (2010). Considering the systematics involved, the solar twin calibration stands as a competitive and model-independent technique which rivals interferometric data in setting the absolute scale, and being affected by virtually no systematics. We also find excellent agreement with the recent interferometric diameters of four giant stars in Huber et al. (2012) and with that of HD122563 at [Fe/H] $= -2.3$ (Creevey et al. 2012), thus providing a positive

test of the IRFM temperatures for giants down to the metal-poor regime.

The IRFM temperature scale by Casagrande et al. (2010) inspired an independent reanalysis of stellar parameters in the Geneva–Copenhagen Survey. Its temperatures are about 80 K hotter than the original GCSIII temperatures, inducing various effects in the interpretation of the data (C11). Discriminating between the two scales was one of the motivations behind this work. We proved that *direct* application of the IRFM yields temperatures in very good agreement with interferometry (within $15-30$ K) when the latest, more accurate interferometric data are used. Such a clear cut conclusion *on the zero-point* of the T_{eff} scale is hard to reach when testing only colour calibrations necessary e.g. for large photometric surveys like the Geneva–Copenhagen Survey. With the additional scatter and metallicity dependence inevitably introduced by colour–metallicity–T_{eff} relations, we find that the two Strömgren scales in GCSIII and C11, are respectively, on the cool and hot side of the interferometric scale – which itself can somewhat change with the adopted compilation of data. It is however encouraging that the agreement is within ± 50 K or better, which is in fact about the 1 per cent accuracy we are striving for.

Nevertheless, colour–T_{eff} relations have high internal consistency, independently on the angular size of stars. It is shown throughout this paper that the comparison between photometric and interferometric effective temperatures as a function of angular diameters is in fact able to reveal trends in interferometric measurements at the smallest diameters. With a critical assessment of angular diameters available in literature, we thus conclude that currently for stars with $\theta \lesssim 1$ mas particular caution must be used, as systematics are seen

to plague some specific interferometric data sets. This must be kept in mind e.g. when discussing discrepancies between models and observations of barely resolved stars.

In particular, interferometry alone is often not enough to perform conclusive tests, other constraints being mandatory. This is crucial for e.g. for ensuring the correct calibration of current and future large surveys, be they photometric or spectroscopic. In this spirit, we have already used more than one method to test effective temperatures in our past investigations (solar twins, line depth ratio and absolute spectrophotometry). Here, we present a new one to gauge the temperature and diameter scale, by combining astrometric distances and asteroseismic radii to the IRFM. As of now, the method is tentative, yet it already suggests that significantly different temperatures (100 K cooler or hotter than the present IRFM scale) are disfavoured, and it holds promise in the view of the upcoming *Gaia* distances and all-sky asteroseismic missions (e.g. *K2*, Chaplin et al. 2013; *TESS*, Ricker et al. 2010). For instance, since the adopted T_{eff} and diameter scales are now tested on nearby, reddening free stars, and astrometric distances and seismic radii are reddening independent, a possible application will be to derive the values of reddening upon which each IRFM angular diameter agrees with that estimated from its seismic radius and astrometric distance, thus building 3D extinction maps of the Galaxy on a star-by-star basis.

ACKNOWLEDGEMENTS

REFERENCES

Allende Prieto C., Asplund M., García López R. J., Lambert D. L., 2002, ApJ, 567, 544
Alonso A., Arribas S., Martinez-Roger C., 1996a, A&AS, 117, 227
Alonso A., Arribas S., Martinez-Roger C., 1996b, A&A, 313, 873
Andersen J., 1991, A&AR, 3, 91
Asplund M., García Pérez A. E., 2001, A&A, 372, 601
Asplund M., Grevesse N., Sauval A. J., Scott P., 2009, ARA&A, 47, 481
Aufdenberg J. P., Ludwig H. G., Kervella P., 2005, ApJ, 633, 424
Bazot M. et al., 2011, A&A, 526, L4
Bell R. A., Gustafsson B., 1989, MNRAS, 236, 653
Bessell M. S., 1990, A&AS, 83, 357
Bigot L., Kervella P., Thévenin F., Ségransan D., 2006, A&A, 446, 635
Blackwell D. E., Lynas-Gray A. E., 1994, A&A, 282, 899
Blackwell D. E., Shallis M. J., 1977, MNRAS, 180, 177
Blackwell D. E., Shallis M. J., Selby M. J., 1979, MNRAS, 188, 847
Blackwell D. E., Petford A. D., Shallis M. J., 1980, A&A, 82, 249
Blackwell D. E., Petford A. D., Arribas S., Haddock D. J., Selby M. J., 1990, A&A, 232, 396
Blackwell D. E., Lynas-Gray A. E., Petford A. D., 1991, A&A, 245, 567

Bohlin R. C., 2007, in Sterken C., ed., ASP Conf. Ser. Vol. 364, The Future of Photometric, Spectrophotometric and Polarimetric Standardization. Astron. Soc. Pac., San Francisco, p. 315
Boyajian T. S. et al., 2012a, ApJ, 746, 101
Boyajian T. S. et al., 2012b, ApJ, 757, 112
Brown R. H., Twiss R. Q., 1958, Proc. R. Soc. A, 248, 222
Carpenter J. M., 2001, AJ, 121, 2851
Carter B. S., 1990, MNRAS, 242, 1
Carter B. S., Meadows V. S., 1995, MNRAS, 276, 734
Casagrande L., 2008, Phys. Scr. T, 133, 014020
Casagrande L., 2009, Mem. Soc. Astron. Ital., 80, 727
Casagrande L., Portinari L., Flynn C., 2006, MNRAS, 373, 13
Casagrande L., Flynn C., Bessell M., 2008, MNRAS, 389, 585
Casagrande L., Ramírez I., Meléndez J., Bessell M., Asplund M., 2010, A&A, 512, A54
Casagrande L., Schönrich R., Asplund M., Cassisi S., Ramírez I., Meléndez J., Bensby T., Feltzing S., 2011, A&A, 530, A138 (C11)
Casagrande L., Ramírez I., Meléndez J., Asplund M., 2012, ApJ, 761, 16
Celis S. L., 1986, ApJS, 60, 879
Chaplin W. J., Miglio A., 2013, ARA&A, 51, 353
Chaplin W. J. et al., 2013, preprint (arXiv:1309.0702)
Chaplin W. J. et al., 2014, ApJS, 210, 1
Chiavassa A., Collet R., Casagrande L., Asplund M., 2010, A&A, 524, A93
Chiavassa A., Bigot L., Kervella P., Matter A., Lopez B., Collet R., Magic Z., Asplund M., 2012, A&A, 540, A5
Code A. D., Bless R. C., Davis J., Brown R. H., 1976, ApJ, 203, 417
Cohen M., Walker R. G., Barlow M. J., Deacon J. R., 1992, AJ, 104, 1650
Cohen M., Wheaton W. A., Megeath S. T., 2003, AJ, 126, 1090
Colavita M. M. et al., 1999, ApJ, 510, 505
Cousins A. W. J., 1980, South Afr. Astron. Obs. Circ., 1, 234
Creevey O. L. et al., 2012, A&A, 545, A17
Cutri R. M. et al., 2003, The IRSA 2MASS All-Sky Point Source Catalog, NASA/IPAC Infrared Science Archive, available at: http://irsa.ipac.caltech.edu/applications/Gator/
Datson J., Flynn C., Portinari L., 2012, MNRAS, 426, 484
Datson J., Flynn C., Portinari L., 2014, preprint (arXiv:1401.1316)
Davis J., Tango W. J., 1986, Nature, 323, 234
Davis J., Ireland M. J., North J. R., Robertson J. G., Tango W. J., Tuthill P. G., 2011, Publ. Astron. Soc. Aust., 28, 58
Demory B. O. et al., 2009, A&A, 505, 205
di Benedetto G. P., 1998, A&A, 339, 858
Dyck H. M., Benson J. A., van Belle G. T., Ridgway S. T., 1996, AJ, 111, 1705
Feltzing S., Bensby T., 2008, Phys. Scr. T, 133, 014031
Glass I. S., 1974, Mon. Notes Astron. Soc. South. Afr., 33, 53
González Hernández J. I., Bonifacio P., 2009, A&A, 497, 497
Gray R. O., Corbally C. J., Garrison R. F., McFadden M. T., Robinson P. E., 2003, AJ, 126, 2048
Hanbury Brown R., Davis J., Allen L. R., 1974, MNRAS, 167, 121
Hekker S. et al., 2009, A&A, 506, 465
Hinkley S. et al., 2010, ApJ, 712, 421
Høg E. et al., 2000, A&A, 355, L27
Holmberg J., Nordström B., Andersen J., 2007, A&A, 475, 519
Holmberg J., Nordström B., Andersen J., 2009, A&A, 501, 941
Huber D. et al., 2012, ApJ, 760, 32
Ireland M. J. et al., 2008, in Schöller M., Danchi W. C., Delplancke F., eds, Proc. SPIE Conf. Ser. Vol. 7013, Optical and Infrared Interferometry. SPIE, Bellingham, p. 701324
Kervella P., Thévenin F., Ségransan D., Berthomieu G., Lopez B., Morel P., Provost J., 2003a, A&A, 404, 1087
Kervella P., Thévenin F., Morel P., Bordé P., Di Folco E., 2003b, A&A, 408, 681
Kervella P. et al., 2008, A&A, 488, 667
King J. R., Boesgaard A. M., Schuler S. C., 2005, AJ, 130, 2318
Lallement R., Vergely J. L., Valette B., Puspitarini L., Eyer L., Casagrande L., 2014, A&A, 561, 91
Leroy J. L., 1993, A&A, 274, 203
Ligi R. et al., 2012, A&A, 545, A5

Magic Z., Collet R., Asplund M., Trampedach R., Hayek W., Chiavassa A.,
    Stein R. F., Nordlund Å., 2013, A&A, 557, 26
Matteucci F., 2003, The Chemical Evolution of the Galaxy. Springer, Berlin
Meléndez J., Ramírez I., 2007, ApJ, 669, L89
Meléndez J., Asplund M., Gustafsson B., Yong D., 2009, ApJ, 704, L66
Meléndez J., Casagrande L., Ramírez I., Asplund M., Schuster W. J., 2010a,
    A&A, 515, L3
Meléndez J., Schuster W. J., Silva J. S., Ramírez I., Casagrande L., Coelho
    P., 2010b, A&A, 522, A98
Menzies J. W., Cousins A. W. J., Banfield R. M., Laing J. D., 1989, South
    Afr. Astron. Obs. Circ., 13, 1
Michelson A. A., Pease F. G., 1921, ApJ, 53, 249
Mozurkewich D. et al., 1991, AJ, 101, 2207
Mozurkewich D. et al., 2003, AJ, 126, 2502
Muñoz Bermejo J., Asensio Ramos A., Allende Prieto C., 2013, A&A, 553,
    A95
Nordgren T. E. et al., 1999, AJ, 118, 3032
Nordlander T., Korn A. J., Richard O., Lind K., 2012, ApJ, 753, 48
Nordström B. et al., 2004, A&A, 418, 989
North J. R. et al., 2007, MNRAS, 380, L80
North J. R. et al., 2009, MNRAS, 393, 245
Pagel B. E. J., 1997, Nucleosynthesis and Chemical Evolution of Galaxies.
    Cambridge Univ. Press, Cambridge
Pease F. G., 1931, Ergebnisse Exakten Naturwissenschaften, 10, 84
Pereira T. M. D., Asplund M., Collet R., Thaler I., Trampedach R., Leenaarts
    J., 2013, A&A, 554, A118
Pinsonneault M. H., An D., Molenda-Żakowicz J., Chaplin W. J., Metcalfe
    T. S., Bruntt H., 2012, ApJS, 199, 30
Porto de Mello G. F., da Silva L., 1997, ApJ, 482, L89

Ramírez I., Meléndez J., 2005a, ApJ, 626, 446
Ramírez I., Meléndez J., 2005b, ApJ, 626, 465
Ramírez I., Meléndez J., Asplund M., 2009, A&A, 508, L17
Ramírez I. et al., 2012, ApJ, 752, 5
Ricker G. R. et al., 2010, BAAS, 42, 459
Rieke G. H. et al., 2008, AJ, 135, 2245
Ruchti G. R., Bergemann M., Serenelli A., Casagrande L., Lind K., 2013,
    MNRAS, 429, 126
Sbordone L. et al., 2010, A&A, 522, A26
Silva Aguirre V. et al., 2011, ApJ, 740, L2
Silva Aguirre V. et al., 2012, ApJ, 757, 99
Sousa S. G., Santos N. C., Israelian G., Mayor M., Udry S., 2011, A&A,
    533, A141
Stello D., Chaplin W. J., Basu S., Elsworth Y., Bedding T. R., 2009, MNRAS,
    400, L80
Takeda Y., Kang D. I., Han I., Lee B. C., Kim K. M., 2009, PASJ, 61, 1165
Torres G., Andersen J., Giménez A., 2010, A&AR, 18, 67
Valenti J. A., Fischer D. A., 2005, ApJS, 159, 141
van Belle G. T., von Braun K., 2009, ApJ, 694, 1085
van Belle G. T., Ciardi D. R., Boden A. F., 2007, ApJ, 657, 1058
van Leeuwen F., 2007, A&A, 474, 653
VandenBerg D. A., Casagrande L., Stetson P. B., 2010, AJ, 140, 1020
von Braun K. et al., 2011, ApJ, 740, 49
White T. R. et al., 2013, MNRAS, 433, 1262
Wielen R., Fuchs B., Dettbarn C., 1996, A&A, 314, 438

This paper has been typeset from a TeX/LaTeX file prepared by the author.